EUROPEAN ORGANIZATION FOR NUCLEAR RESEARCH

LHCb 98-035
RICH
30 January 1998

DEVELOPMENT OF PIXEL HYBRID PHOTON DETECTORS FOR THE RICH COUNTERS OF LHCB

M. Campbell1), F. Formenti1), T. Gys*1), D. Piedigrossi1),
D. Puertolas2), E. Rosso1), W. Snoeys1), K. Wyllie1)

1) CERN, Geneva, Switzerland
2) INFN Section of Rome, Italy

Abstract

The particle identification system proposed for the LHCb experiment is based on RICH counters with three different radiator materials and hybrid photon detectors (HPDs) as a possible readout. Within this framework, one approach to HPD design is the "pixel-HPD". This is based on standard image intensifier geometries that strongly focus the photoelectrons onto a silicon pixel array, bump-bonded to a binary readout chip with matching pixel electronics. This paper reports on the ongoing developments in this field and in particular on the first operation of a 40:11 mm pixel-HPD prototype tube.

To be submitted to Nuclear Instruments and Methods A

---

[*] Corresponding author. Address: EP Division, CERN, CH-1211 Geneva 23, Switzerland.
Phone: ++41 22 767 83 07. Fax: ++41 22 767 32 00. Email: Thierry.Gys@cern.ch

1 INTRODUCTION

The main focus for the photodetectors of the LHCb RICH system (see [1] and references therein) is on hybrid photon detectors (HPDs) which use a silicon detector anode inside a vacuum envelope. A photocathode is deposited on an optical input window in the envelope, and the photoelectron released by an incident photon is accelerated onto the silicon detector by an applied high voltage of ~20 kV (corresponding to ~5000 e^- released in the silicon). Commercially available examples of HPDs exist, but do not fully meet the specific LHCb requirements, in particular the large area coverage (~2.9 m^2) with high active-to-total area ratio(~70 %), small granularity (2×2 mm^2 at the photocathode level)[1] and high speed (25 ns).

The development of the pixel-HPD is being carried out in close collaboration with industry[2]. It is based on a cross-focussing tube design, demagnifying by a factor of ~4 the photocathode image onto a small detector array with O(500 μm) pixels, bump-bonded to a binary readout chip with matching pixel electronics integrated inside the vacuum envelope of the tube. The feasibility of this approach was demonstrated in 1994 by the successful realization of the "ISPA-tube" [2]. The first ISPA-tubes, based on magnetically focussed electron optics, had a one-to-one mapping geometry resulting in a total active surface of 4.8×8.0 mm^2. They have been initially developed to read out small diameter scintillating fibres for particle tracking (see [3] and references therein). They have also been shown to be an excellent detection tool for biomedical applications (see [4] and references therein).

The performance of cross-focussed, or first generation, image intensifiers is well known [5]. In particular, these devices can reach a limiting spatial resolution of up to 100 line pairs per mm (lp/mm) (or equivalently 10 μm)[3]. Their image distortion, caused by variations of the linear demagnification along the radial distance, does not generally exceed 10 % at the edge, and can be corrected off-line. These tube geometries are robust to external electric and magnetic field perturbations [6]. In parallel, small pixels with bump-bond connections to the front-end electronics lead to small capacitances (giving low noise and high speed) and a compact anode structure with a limited number of feedthroughs. Binary electronics have low power consumption (a few 100 μW per channel) and are consequently well adapted to implementation in a vacuum tube. In addition, they are compatible with the demanding bake-out cycles needed for high-quality photocathodes.

---

[1] Recent proposals have suggested changing this granularity to 2.5×2.5 mm^2. Our calculations are based on a granularity of 2×2 mm^2.

[2] Delft Electronische Producten (DEP) B.V., Roden, The Netherlands.

[3] The limiting spatial resolution corresponds to an image contrast of 3 % and is expressed in lp/mm. The inverse of its value is the full width at half maximum of the point spread function expressed in μm.

2 40:11 MM TUBE PROTOTYPE

2.1 Design considerations

A cross-focussed pixel-HPD prototype tube has been developed and is shown schematically in figure 1. Its input window is made of quartz and is 40 mm in active diameter. The photocathode is deposited on a curved, spherical surface. The photoelectron image is focussed onto the flat surface of a silicon detector chip mounted in the die cavity of a standard ceramic carrier[1]. The silicon detector is a pixelated structure bump-bonded to the LHC1 chip [7]. This comprises an array of 128×16 pixels of 50×500 μm^2 giving a total silicon active surface of 6.4×8.0 mm^2. The anode active diameter, corresponding to the diagonal of the chip, is thus ~11 mm. Taking into account the demagnification ratio of ~4, the detection surface is 16 times larger at the photocathode level (~25×32 mm^2), and the input granularity is 0.2×2.0 mm^2. The tube can be operated up to 20 kV.

The LHC1 chip is being used for charged particle tracking detectors in heavy ion experiments. Each detector pixel is individually connected to a readout chain containing amplifier, discriminator with adjustable threshold, globally adjustable delay line with local fine-tuning, coincidence logic and memory. Every cell can be individually addressed for electrical tests and masking. The analogue power consumption is below 50 μW per channel. This chip permits measurements to be made with short peaking time (100 ns), close to the LHC requirement. However, the lowest comparator threshold of 4000 e^- and its spread of 1000 e^- are too high for HPD application. In addition, the pixel size of 50 μm is unnecessarily small, leading to charge sharing between pixels (see ref. [8] and § 2.3.1) and low yields for bump bonding (see § 4).

2.2 Electron optics simulation

In a cross-focussed image tube, the boundary of the electron optics is shaped to produce a centrally-symmetric field (to a close approximation) between the cathode spherical surface and the cathode aperture. This aperture forms a divergent lens that modifies the location and the radius of the image sphere of the centrally-symmetric lens [5]. Photoelectrons are sharply focussed on the silicon detector by the combination of these two lenses, forming an inverted image.

The electron optics have been simulated at DEP and at CERN. The electric field distribution has been calculated with the POISSON package [9] which can solve electrostatic problems with cylindrical symmetry. The resulting voltage distribution inside the tube is shown in figure 2. The equipotential lines range from –15 kV (at the cathode level) to 0 kV (at the chip) with a 1 kV step. Electron trajectories are obtained by solving the equation of motion with a time-step method [10]. Figure 3 shows a set of such trajectories for meridional photoelectrons (ie drifting in a plane containing the tube axis) emitted normal to the cathode surface and at ± 45 ° to the normal. Their initial kinetic energy is 1.0 eV (corresponding to an initial velocity of 0.6 m/μs. In the text below, initial velocities will be expressed in eV). On the top picture of figure 3, the r axis has been stretched for clarity (ie in this representation,

---

[1] Kyocera Fine Ceramics, Japan.

angles are not conserved). As expected from the cylindrical symmetry, meridional electrons stay in this plane. Consequently, the (x,y) projection (bottom picture of figure 3) is a straight line. This simulation gives a demagnification of 0.222 on-axis, and 0.254 at the edge (corresponding to an edge distortion of 8.0 %). The simulated point-spread function (PSF) of the tube near the axis is shown in figure 4. It is generated from a set of photoelectrons whose velocity spectrum is Maxwellian with a most probable velocity of 0.25 eV and a maximum velocity of 1 eV. This spectrum corresponds to a monochromatic blue photon illumination (3 eV in energy or 415 nm in wavelength) detected by an S20 multialkali photocathode (2 eV in cut-off energy or 620 nm in wavelength) [11]. The emission angle is assumed to follow a Lambert cosine distribution. The full width at half maximum of the PSF is equal to 32 μm, corresponding to a limiting resolution of 30 lp/mm.

2.3 Preliminary experimental results

Two successful encapsulations of an LHC1 chip in a tube were carried out at DEP in December 1997. The photocathode response was measured by DEP and was stable over two weeks. Both tubes were tested up to 20 kV without problems. They were delivered to CERN in January 1998 and no change was seen in the electrical performance of the electronics compared to test results prior to encapsulation. The detector leakage currents were the same. Figure 5 is a photograph of one of the tubes attached to the electronics support board. The cable protruding from the tube is for the high voltage. Figure 6 shows the silicon anode at three stages of mounting on the tube base.

2.3.1 Photoelectron response

The tubes have been tested using a procedure described in detail in reference [8]. Measurements were carried out with the tubes in a light-tight box (figure 7). The light source was 20 cm distant and consisted of a blue LED operated in pulsed mode.

The tube support board was connected to the LHC1 readout system. Signals from the backplane of the silicon detector anode were read out with an electronics chain consisting of an ORTEC 142A preamplifier, an ORTEC 579 CR-RC fast-filter amplifier with time constants of 200 ns (CR) and 500 ns (RC) and a SILENA multi-channel analyser. This allowed measurement of the signal spectrum due to photoelectrons from the backplane of the detector. Figure 8 shows a typical spectrum at a detector bias of 55 V and a tube high voltage of 19.5 kV, and the peaks for 0, 1, 2, 3 and 4 photoelectrons are clearly visible. A fit [12] was made to each spectrum, and the average number of photoelectrons, μ, was calculated with a precision of 5 %. Spectra were measured at regular intervals during data-taking to monitor drifts in the output intensity of the LED. The amplifiers were calibrated with a test input and results indicate that the signal created by a single photoelectron is 4600 e^-, with a 5 % uncertainty. This is consistent with a tube high voltage of 19.5 kV and losses of about 2 kV in the backplane of the detector.

The detector was then read out by the pixel chip operating at a threshold setting of 2450 mV (corresponding to a discriminator bias current of 16.2 μA). 223 noisy pixels were masked. For a constant tube high voltage of 19.5 kV, the detector bias was scanned from 35 to 90 V. At each point in the scan, the fraction of events where one or more pixels fired was calculated. From Poisson statistics, this fraction is equal to $(1-e^{-\mu'})$ where μ' is the average number of firing pixels. Figure 9 shows the results of the scan. 20 keV photoelectrons are stopped within the first few microns of silicon and this is illustrated in the bias scan by the detector becoming sensitive to photoelectrons at ~45 V, corresponding to full depletion. Over-depleting the detector results in a large increase in efficiency. The maximum detector bias was limited to 90 V because of the risk of avalanche breakdown, but a small increase in efficiency would result from a further increase in bias. The data illustrate a particular limitation of the structure of this detector for photoelectrons with 19.5 keV energy. Holes created at the backplane drift across 300 μm of silicon but will simultaneously diffuse in the lateral dimensions and be shared amongst pixels, an effect which is enhanced by the 50 μm pitch. For higher bias voltage, and hence higher electric field, the drift time is decreased, the lateral diffusion is restricted and the charge sharing is reduced. However, at a threshold of ~4000 e^-, the loss of just a few hundred electrons due to charge sharing will decrease the efficiency. Measurements of the backplane spectrum at 55 V and at 90 V are identical, which shows that there is no increase in the amount of charge created at higher bias voltage. There is only a decrease in the time for it to drift to the opposite side of the detector.

A similar scan was carried out, this time varying the tube high voltage whilst maintaining a constant detector bias of 90 V. The backplane spectrum was measured before the scan and is shown in figure 10. The average number of firing pixels as a function of the tube high voltage was calculated and the results are shown in figure 11. The data show the detector becoming sensitive at about 13 kV, and the efficiency increasing rapidly above 17 kV. It is still increasing at the maximum operating point of 19.5 kV.

The ratio of the average number of firing pixels, μ', to the average number of photoelectrons, μ, is the efficiency of the detector to single photoelectrons, since the probability of a pixel being hit by two or more photoelectrons is negligible ($<10^{-6}$). μ was measured to be 1.40 just before the detector bias scan, and 1.75 just before the high voltage scan. The corresponding maximum values of μ' were 0.34 and 0.38. Before the efficiency can be calculated, corrections have to be made to the values of μ and these are described in the following. Not all of the pixels in the matrix were sensitive to single photoelectrons. The measurements made at 90 V detector bias and 19.5 kV indicated that 1400 different pixels were firing during each run. This we take as the number of sensitive pixels, and is 68 % of the matrix. The remaining pixels were electrically masked (11 %), obscured by the overlapping diaphragm (2 % - see footnote of § 2.3.2) or had high thresholds or poor bump bonding (19 %). This maximum of 1400 sensitive pixels was further supported by measurements with an electrical test input across calibration capacitors connected to the pixel pre-amps. The amplitude of this test signal was varied until 1400 pixels fired. Using a value for the test capacitance of ~15fF [13], this test input injects 5100 e^- into the front-end electronics. This is in reasonable agreement with the calibration of the backplane signal for one photoelectron of 4600 e^-. The 10 % discrepancy is currently being investigated. An additional correction arises from backscattering at the silicon surface. Around 20 % of photoelectrons will be backscattered and deposit on average only half of their energy in the detector [14]. This contributes to the continuum seen in the backplane spectrum but also means that the signal from these photoelectrons will be too low to reach the pixel discriminator threshold. Even a loss of a few hundred electrons due to scattering would decrease the efficiency since the threshold is very close to the maximum possible signal. This is similar to the charge sharing effect. Combining the fraction of sensitive pixels and the backscattering effect gives a correction factor for μ of 0.68 × 0.8 = 0.54. The corrected values of μ are thus 0.76 and 0.95.

The amount of charge sharing has been estimated using equations derived in [15]. Assuming a depletion voltage, U_D, of 45 V, the hole transit time, t, can be calculated for different bias voltages, U. Charge created at a point on the backplane will diffuse and appear as a Gaussian distribution on the junction (pixel) side of the detector with a standard deviation σ. Table 1 lists the values of t and σ for three different values of U. We then assume that a pixel becomes inefficient if 10 % of the charge is lost to the adjacent pixel. This corresponds to ~500 e^- signal which is ~2kV of acceleration potential. The assumption is justified by the lower efficiency achieved at 2kV below the maximum tube high voltage, as shown in figure 11. When the cloud centre is 1.3 σ away from the pixel boundary, 10 % of the charge is collected by the adjacent pixel according to the error function formula. Thus at this threshold, the sensitive fraction of the pixel area, *f*, is given by

$$f = \frac{[50 - (2 \times 1.3\sigma)] \times [500 - (2 \times 1.3\sigma)]}{50 \times 500}$$

The results in Table 1 show that at 90 V bias, *f* is 53 %. This estimate is a final correction to the values of μ, which now become 0.40 and 0.50. The corrected efficiencies (= μ'/ μ) are therefore 85 % and 76 %. The discrepancy between the two efficiencies is due to the error in the average number of photoelectrons given by the fit.

U [V]	t [ns]	σ [μm]	*f* [%]
46	100	17	9
55	51	13	33
90	24	9	53

Table 1

2.3.2 Imaging properties

A 5 mm-thick mask is used to produce a reference image (fig. 7). It consists of a square lattice of circular holes, each 2 mm in diameter and 4 mm distant from their neighbours. This pattern is placed in contact with the flat input surface of the quartz window of the tube. For studies of imaging properties, the LED intensity has been increased such as to produce an image in a short enough period of time.

The output image of the test pattern is reproduced in figure 12. The holes are clearly visible. The circle indicates the image of the mask hole which is aligned with the tube axis[1]. From the vertical projection (top picture of figure 13) and horizontal projection (bottom picture of figure 13), one deduces that the maximum of the LED light distribution is approximately situated at row 30, column 5. Horizontal projections of columns 2 to 4 (top picture), columns 4 to 6 (middle picture) and columns 6 to 8 (bottom picture) are shown in figure 14. A fit has been made to the holes on these projections (solid curves). The fitting function is of the form

$$\sqrt{r^2 - (y - y_0)^2}$$

This corresponds to the projection of a disk with radius r and centre (x_0, y_0). The average hole separation is ~1 mm and the average hole radius r ~0.25 mm, confirming the demagnification factor of ~4. An edge distortion is visible on the top part of figure 12. It is most likely due to the spherical shape of the photocathode surface and to the tube electron optics properties and remains to be analyzed in detail.

3 LARGE TUBE DEVELOPMENTS

The present 40:11 mm prototype tube has been manufactured with standard parts and its active area (~55 %) is not optimal. To increase this area, larger tubes are under development. The two key factors are the mechanical restrictions related to the input window sealing technology, and the performance of the electron optics near the edge of the tube. Preliminary design studies indicate that the desired active-area fraction (~80 %) can be achieved. The present baseline dimensions of this tube (schematically shown in figure 12) are a 72 mm active photocathode diameter (80 mm total), and an 18 mm active anode diameter. (i.e. a linear demagnification by 4). With an input granularity of 2×2 mm^2, the tube would contain 1024 channels. The next step of this development will be to produce such a tube with a phosphor screen anode coupled to a CCD camera, in order to test its photocathode and focussing properties. A second version of the tube would be equipped with a 61 pixel silicon detector identical to the one used in the LHCb RICH prototype set-up [16]. The anode would eventually be mounted with a silicon chip containing 32×32 channels each 500×500 μm^2 in size (see § 4 below).

4 PIXEL ELECTRONICS DEVELOPMENTS

A front-end binary pixel chip for the LHCb RICH must meet stringent requirements.

Firstly, the chip must correctly discriminate hits and tag them with a specific bunch crossing. This requires the front-end amplifier to have a shaping time of $\leq$ 25 ns and the subsequent discriminator to apply a threshold of $< 2000\ e^-$ with a pixel-to-pixel RMS spread

---

[1] An error was made during the mounting of the chip in the die cavity of the ceramic carrier. This resulted in an offset of the silicon detector with respect to the tube axis. The top right corner of the silicon detector is therefore obscured by the diaphragm placed above it.

of < 200 e^-. Both of these requirements have been reached in recent developments for other applications. A threshold of 1400 e^- with an RMS of 80 e^-, incorporating a 3-bit adjustment per pixel, has been achieved on a chip designed for X-ray photon imaging [17]. An additional test chip, fabricated in a commercial 0.5 μm technology, has a peaking time of 25 ns and exhibits a timewalk of < 25 ns for signals 100 e^- above threshold [18]. Its timing resolution therefore meets the LHCb requirement. The analogue power consumption is below 50 μW per channel. In addition, the chip has been demonstrated to be radiation tolerant up to 600 kRad, which is beyond the integrated dose predicted in the RICH detectors. This radiation tolerance has been achieved using special layout techniques described in [18].

Secondly, the nature of the experiment places strong demands on the digital circuitry which stores the discriminated signals. High occupancy (maximum 5-10%), high level-0 trigger rate (mean 1 MHz) and a long level-0 latency (3.2 μs) require that the chip is capable of storing a large number of hits for a long period and is able to transfer data at a high rate to minimise dead-time. A digital architecture specifically for the RICH is currently being studied and simulated, and is a development of a global architecture for LHCb outlined in [19]. The hit-storage will be implemented as a pipeline or a series of counters whose storage time matches the trigger latency. Following the trigger coincidence, data will be stored in a FIFO memory with the capacity for 16 events. This reduces losses caused by statistical fluctuations in the trigger rate.

The LHCb RICH pixel chip is currently foreseen as consisting of 32 rows and 32 columns of 500×500 μm^2 pixels. The pixel size is substantially larger than in the devices used for prototype tubes described above, reducing the effect of charge sharing between pixels and allowing the necessary digital circuitry to be integrated into the cell. The number of columns is common to the global LHCb architecture [19], and allows the data from a chip to be read out in 800 ns through 32 parallel lines at a rate of 40 MHz. Simulations show that a 16-deep FIFO read out every 800 ns will reduce the dead time to 0.02%.

An important development is the implementation of pixel circuitry in a 0.25 μm technology, which is currently under investigation as part of the pixel programme for ALICE [20]. Such a technology not only offers a higher feature density but also allows the use of multiple metal layers, which will be beneficial in shielding analogue circuitry from large, digital voltage swings. Both of these aspects are attractive to LHCb. The bump-bonding procedure is also under study in collaboration with a number of other pixel projects. Yields of bump-bonding assemblies from one vendor have so far been poor, and the aim of this investigation is to improve the yield to levels acceptable for large scale production. The study involves close collaboration with industry and is also intended to identify other possible vendors.

5 SYSTEM ASPECTS

The front-end electronics of LHCb extend beyond the level-1 trigger-accept and conclude with the multiplexing of a number of detector modules onto a high speed link to the DAQ. An initial architecture for a RICH pixel system is shown in figure 16, which illustrates the simplicity of a scheme where data are in binary form. The estimates of buffer-size and bandwidth are for a worst-case scenario of 10 % occupancy.

Following a level-0 trigger-accept, data from one HPD (1 k pixels) are transferred along a 32-wide twisted pair cable (one pair per column) at a rate of 40 MHz. These are stored in a level-1 buffer as 32-bit words (1 word = 1 row). The capacity of this buffer is determined by the level-1 latency of ~256 μs. For a mean level-0 trigger rate of 1 MHz, the buffer must be large enough to store 256 events and thus requires 256×32 = 8 k words of memory.

The level-1 rate is ~40 kHz. Therefore, after a level-1 accept, data must be transferred at ≥ 1.28 MHz and then zero-suppressed. Each hit will be encoded as a 10 bit word representing the pixel address. For 10 % occupancy (~100 hits per event per HPD), 100 words of data need to be transferred every 25 μs, requiring a rate of 4 Mword/s. Multiplexing 16 HPDs onto a serial link to the DAQ would require an additional 4 bits per hit to indicate the HPD address. The bandwidth required is thus 14 bits × 4 Mword/s × 16 = 0.896 Gbit/s, which is satisfied by a 1 Gbit/s link. For an LHCb RICH detector comprising ~500 HPDs, 32 such data links would be needed.

The scheme could be implemented using commercially available components, such as standard RAM for the level-1 memory and FPGAs to carry out the zero-suppression. However, these electronics may be placed close to the detector where they will be subject to radiation damage. Radiation levels at possible locations for these components are currently being investigated.

6 CONCLUSIONS

Two cross-focussed HPD prototypes with fast (100 ns) pixel readout have been manufactured. Their absolute efficiency at detecting single photoelectrons has been measured. Corrections due to insensitive pixels, backscattering and charge sharing have been applied and result in an efficiency of 80 %. The 20 % inefficiency is yet to be understood and requires a more precise examination of the correction factors above and of the behaviour of the chip. The electron optics behave as expected and confirm the principle of demagnifying a photoelectron image onto a small silicon area.

The improved performance of pixel electronics developed for other applications can now meet the analogue front-end requirements of LHCb. In particular, their lower discrimination threshold suggests that single photon detection efficiencies will be close to optimum. Detailed simulations of the digital circuitry required within an LHCb pixel cell are currently underway, with the aim of designing a specific chip for encapsulation within large tubes with high active area. In parallel, a programme to improve the bump-bonding yield has been initiated in collaboration with other pixel projects. The system requirements of a binary RICH readout have been estimated and highlight the simplicity of such a scheme. The implementation is now under study.

Acknowledgements

The authors acknowledge H.-J. Hilke for his support and the industrial collaborators for their efficient contribution. They are grateful to E. Heijne, spokesman of the CERN RD19 collaboration which developed the LHC1 chip and to M. Letheren, leader of the CERN microelectronics group. They thank H. Leutz and C. D’Ambrosio for discussions and O. Ullaland for comments. H. Beker, E. Cantatore, E. Chesi, P. Martinengo and M. Sanchez were involved in software and hardware for the readout electronics. M. Luptak tested the LHC1 chips on the probe station. B. Cantin and D. Fraissard improved the mechanical test set-up. Some bake-out and outgassing tests of the chips were performed at CERN thanks to C. Benvenuti and P. Chiggiato. The pulsed LED driver circuit was designed by P. Nappey and realized by J.-L. Garavel.

References

[1] The LHC-B Collaboration, “Status and plan of R&D for the RICH detectors of LHC-B”, CERN/LHCC 96-38, LHC-B 96-10/LHCC 96-03, 23 October 1996.

[2] T. Gys et al., Nucl. Instr. and Meth. A 355 (1995) 386.

[3] C. D’Ambrosio et al., IEEE Trans. Nucl. Sci., vol. 43, 3 (1996) 2127.

[4] D. Puertolas et al., IEEE Trans. Nucl. Sci., vol. 44, 5 (1997) 1747.

[5] I.P. Csorba, “Image Tubes”, Howard W. Sams & Co., 1985.

[6] T. Gys and D. Piedigrossi, “Performance of electrostatically-focussed image intensifier tubes in low magnetic fields”, LHC-B/97-026, 14 November 1997.

[7] E. Heijne et al., Nucl. Instr. and Meth. A 383 (1996) 55.

[8] T. Gys et al., Nucl. Instr. and Meth. A 387 (1997) 131.

[9] C. Iselin, “Solution of Poisson’s or Laplace’s equation in two-dimensional regions”, CERN Program Library long write-up T604, 1984.

[10] T. Seidel, “Calculation of Photoelectron Paths in Cylindrical Coordinates”, CERN EF/IN internal report, 1990. Program upgraded by T. Gys.

[11] G. Wendt, “Sur le pouvoir séparateur du convertisseur d’images à champs homogènes électrostatique et magnétique”, Ann. Radioélectr. 10, 39 (1955) 74.

[12] C. D’Ambrosio et al., Nucl. Instr. and Meth. A 338 (1994) 389.

[13] M. Campbell and B. Mikulec, private communication.

[14] E.H. Darlington, J. Phys. D 8 (1975) 85.

[15] E. Belau et al., Nucl. Instr. and Meth. 214 (1983) 253.

[16] E. Albrecht et al., “First observation of Cherenkov ring images using hybrid photodiodes”, submitted to Nucl. Instr. and Meth. A.

[17] RD19 Status Report on Activities in 1996-7, CERN/LHCC 97-59, LEB Status Report/RD19, 10 October 1997.

[18] W. Snoeys et al, “Demonstration of Adapted Layout Techniques for Increased Radiation Tolerance of Circuits in Commercial Submicron Technologies”, submitted to IEEE Nuclear and Space Radiation Effects Conference, Newport Beach, California, USA, July 20-24 1998.

[19] J. Christiansen, “An overview of the LHCb experiment and its electronics”, Proceedings of the Third Workshop on Electronics for LHC Experiments, CERN/LHCC/97-60, 21 October 1997.

[20] ALICE Technical Proposal, CERN/LHCC/95-71, LHCC/P3, 15 December 1995.

Figure captions

Fig. 1 Schematic design of a 40:11 mm pixel-HPD prototype tube. The electron optics.is based on a diode structure with cross-focussing. On the anode is mounted the LHC1 chip comprising 2048 pixels and their associated front-end electronics.

Fig. 2 Electric potential distribution in the tube as calculated by POISSON. The photocathode voltage is –15 kV, the phosphor is at ground. The equipotential lines are drawn every 1 kV.

Fig. 3 Radial coordinate and (x,y) transverse projection of the calculated photoelectron trajectories for normal tube operation. The vertical axis r of the top picture is stretched for clarity.

Fig. 4 Simulated point spread function for an emission point 5 mm distant from the tube axis. The full width at half maximum is equal to 32 μm (~30 lp/mm).

Fig. 5 Photograph of the 40:11 mm pixel-HPD prototype tube connected to a printed circuit board via a standard pin grid array socket.

Fig. 6 Photograph showing the anode construction phases. The bare LHC1 chip (right) is mounted and wire bonded in a pin grid array ceramic carrier (middle) on which a Kovar flange has been brazed (left).

Fig. 7 Schematic experimental set-up. The tube is placed in a light-tight box and exposed to a weak light source consisting of a blue LED operated in pulsed mode. For electron optics tests, the photocathode window is covered with a test mask.

Fig. 8 Backplane spectrum recorded before the detector bias scan. A fit to the data is indicated by the solid line and yields a photoelectron average of 1.40.

Fig. 9 Average number of firing pixels as a function of detector bias voltage. The tube high voltage was 19.5 kV.

Fig. 10 Backplane spectrum recorded before the tube high voltage scan. A fit to the data is indicated by the solid line and yields a photoelectron average of 1.75.

Fig. 11 Average number of firing pixels as a function of tube high voltage. The silicon detector bias was 90 V.

Fig. 12 Output image of a 5 mm thick test mask consisting of a square lattice of circular holes 2 mm in diameter and 4 mm distant from their neighbours. The resulting hole separation on the pixel detector is ~1 mm, owing to the demagnification factor of ~4 given by the electron optics. The circle indicates the image of the mask hole which is aligned with the tube axis. An image distortion is visible on the top part of the picture and is most likely due to the spherical shape of the photocathode surface and to the tube electron optics properties.

Fig. 13 Vertical (top picture) and horizontal (bottom picture) projections of the 2D-histogram of figure 12. The envelope of these projections shows that the LED centre is around column 5, row 30.

Fig. 14 Horizontal projections of columns 2 to 4 (top picture), columns 4 to 6 (middle picture) and columns 6 to 8 (bottom picture). The fits of the holes (solid curves on the pictures) result in a hole separation of ~1 mm and a hole radius of a ~0.25 mm in the pixel array, confirming the electron optics design.

Fig. 15 Schematic design of a large pixel-HPD tube with high active area. The active input diameter is 72 mm (80 mm total) and the anode active diameter 18 mm. For an input granularity of 2×2 mm^2, the tube would contain 1024 channels arranged as a 32×32 pixel matrix.

Fig. 16 System architecture of the front-end electronics for the binary readout of the LHCb RICH counters.

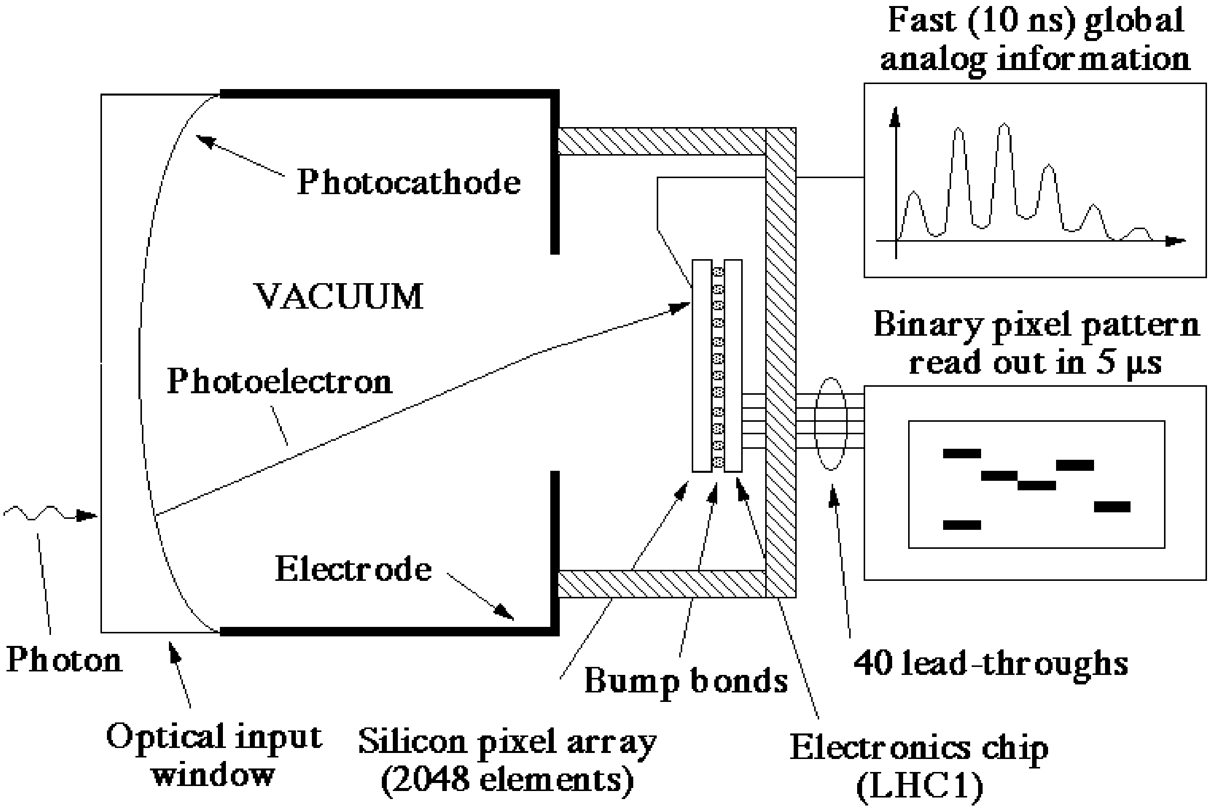
Fast (10 ns) global analog information
Photocathode
VACUUM
Photoelectron
Binary pixel pattern read out in 5 µs
Electrode
Photon
Bump bonds
40 lead-throughs
Optical input window
Silicon pixel array (2048 elements)
Electronics chip (LHC1)

Figure 1

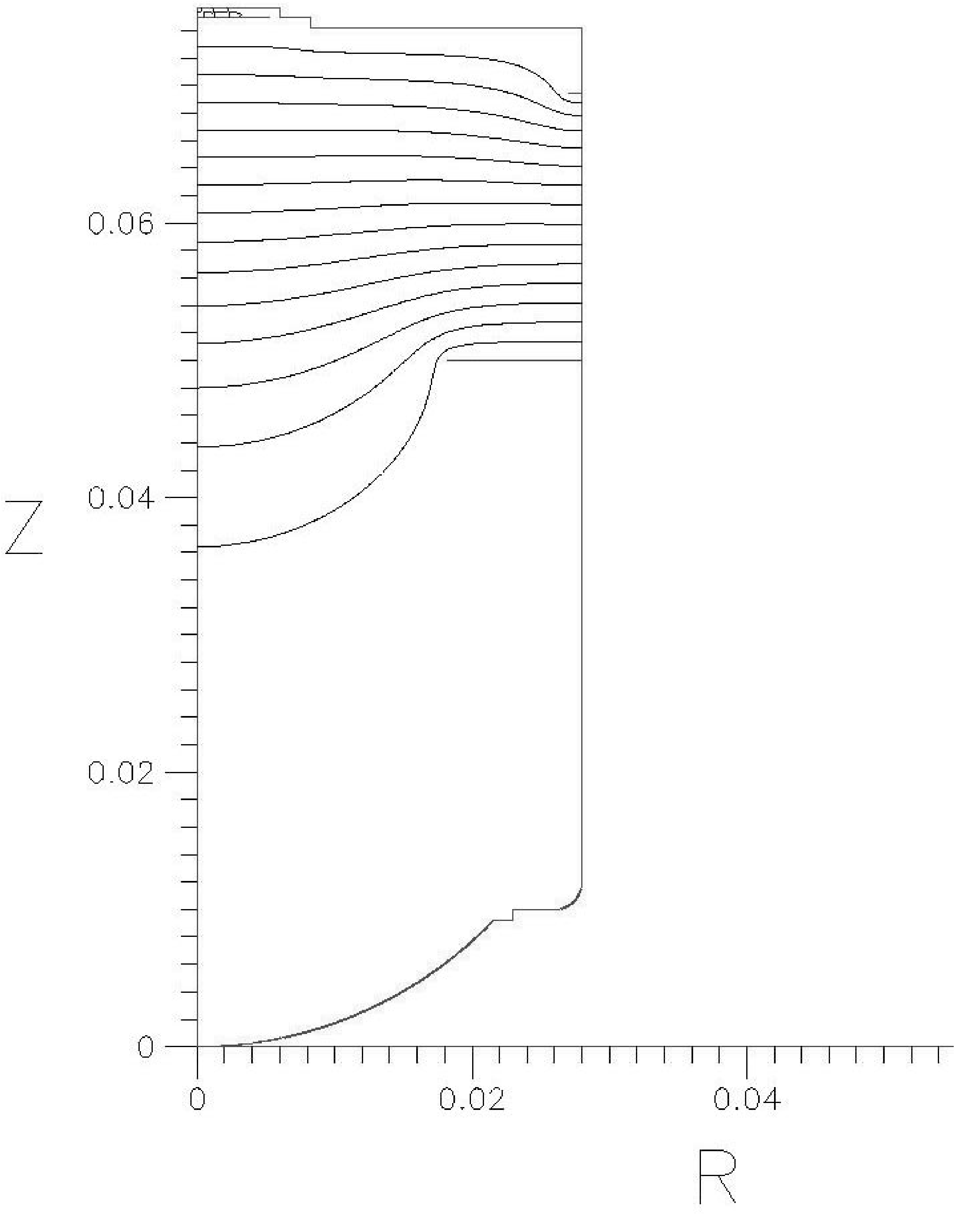

Figure 2

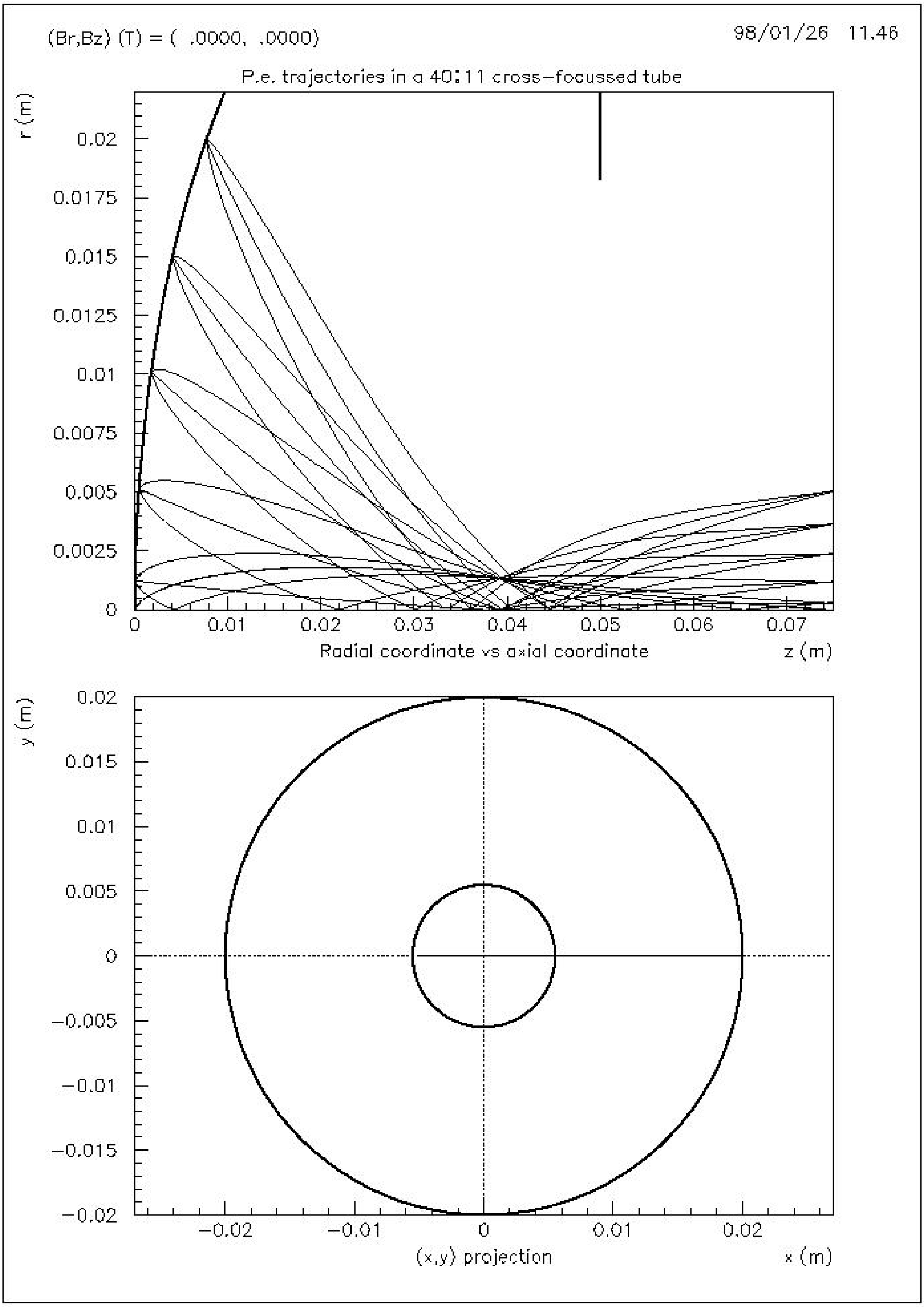
(Br,Bz) (T) = (.0000, .0000)
98/01/26 11.46
P.e. trajectories in a 40:11 cross-focussed tube
r (m)
0.02
0.0175
0.015
0.0125
0.01
0.0075
0.005
0.0025
0
0
0.01
0.02
0.03
0.04
0.05
0.06
0.07
Radial coordinate vs axial coordinate
z (m)
y (m)
0.02
0.015
0.01
0.005
0
−0.005
−0.01
−0.015
−0.02
−0.02
−0.01
0
0.01
0.02
(x,y) projection
x (m)

Figure 3

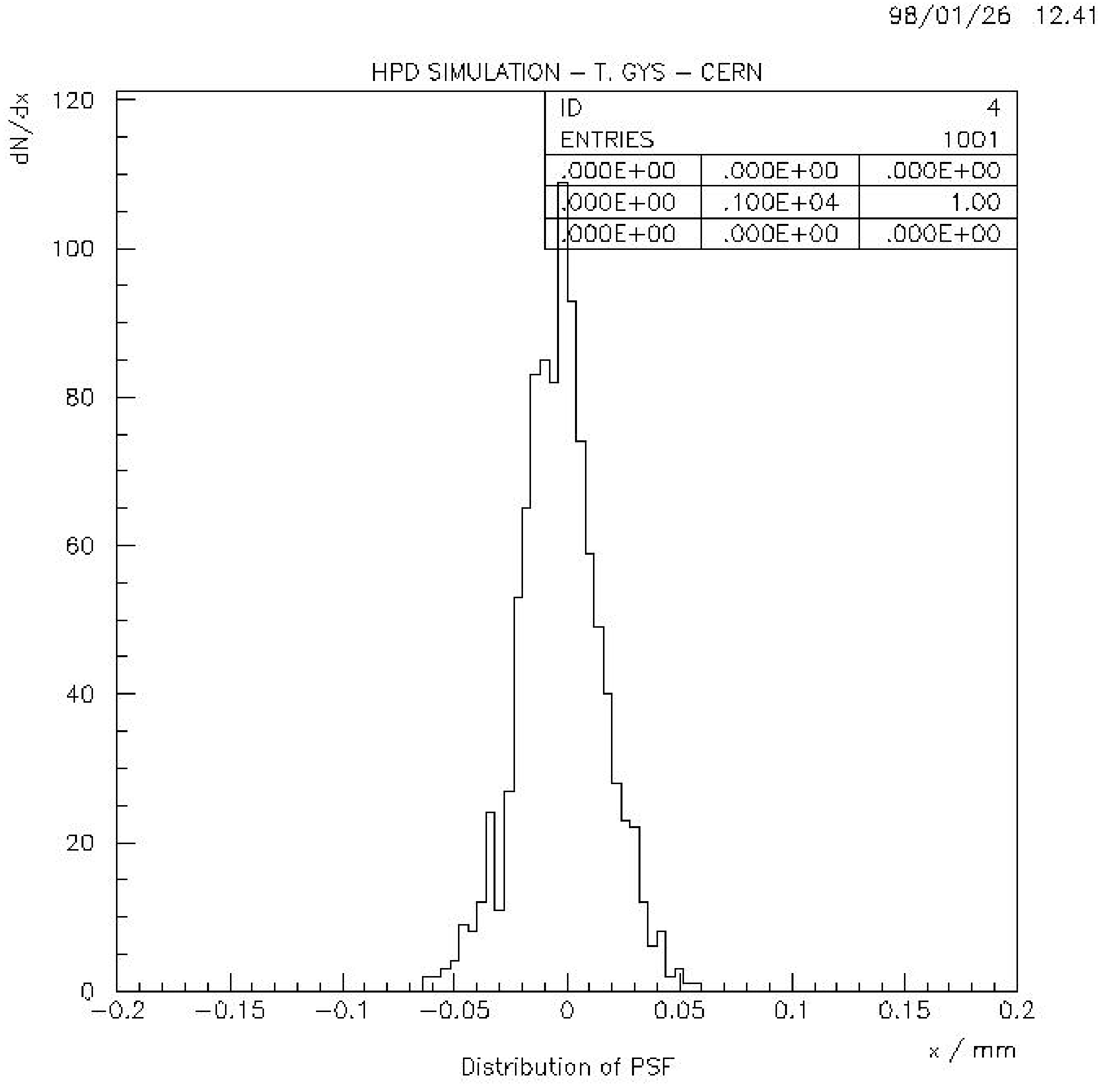
98/01/26 12.41
HPD SIMULATION – T. GYS – CERN
dN/dx
ID 4
ENTRIES 1001
.000E+00 .000E+00 .000E+00
.000E+00 .100E+04 1.00
.000E+00 .000E+00 .000E+00
120
100
80
60
40
20
0
−0.2
−0.15
−0.1
−0.05
0
0.05
0.1
0.15
0.2
x / mm
Distribution of PSF

Figure 4

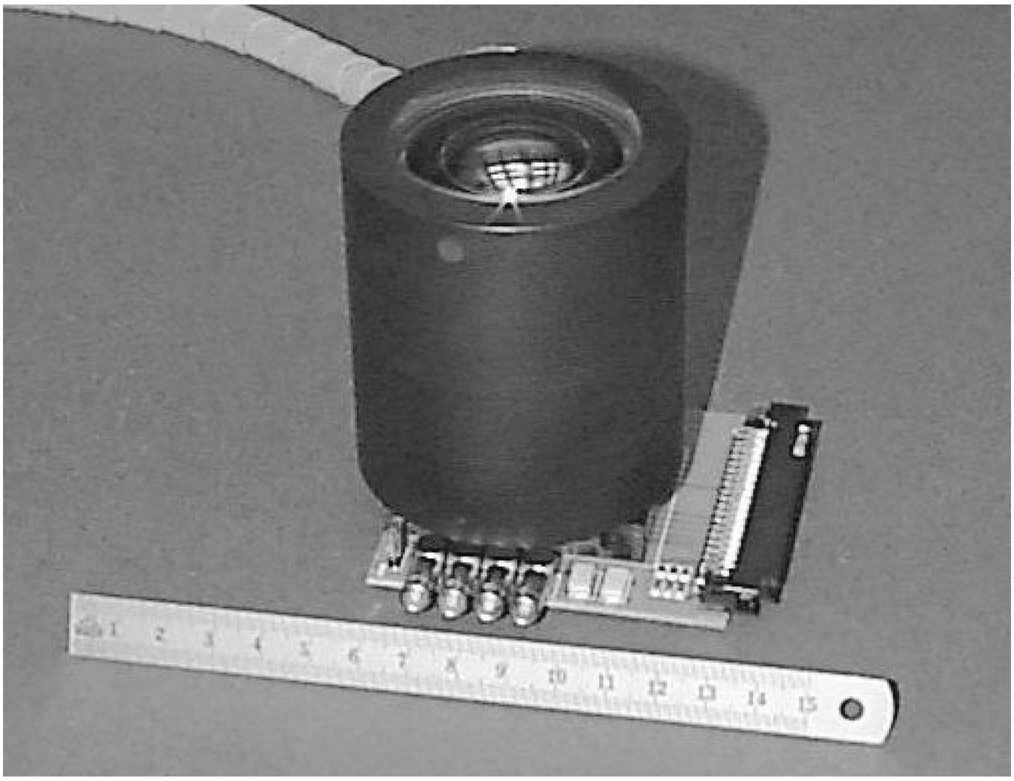

Figure 5

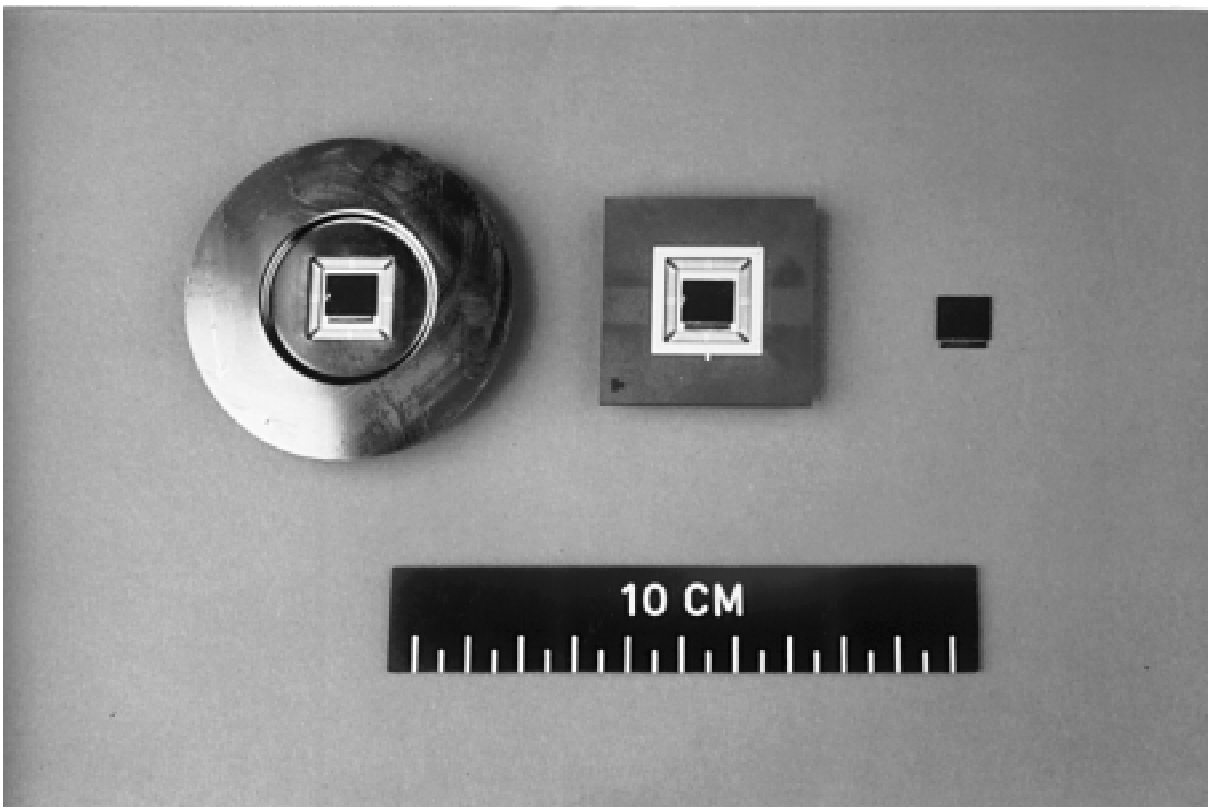

Figure 6

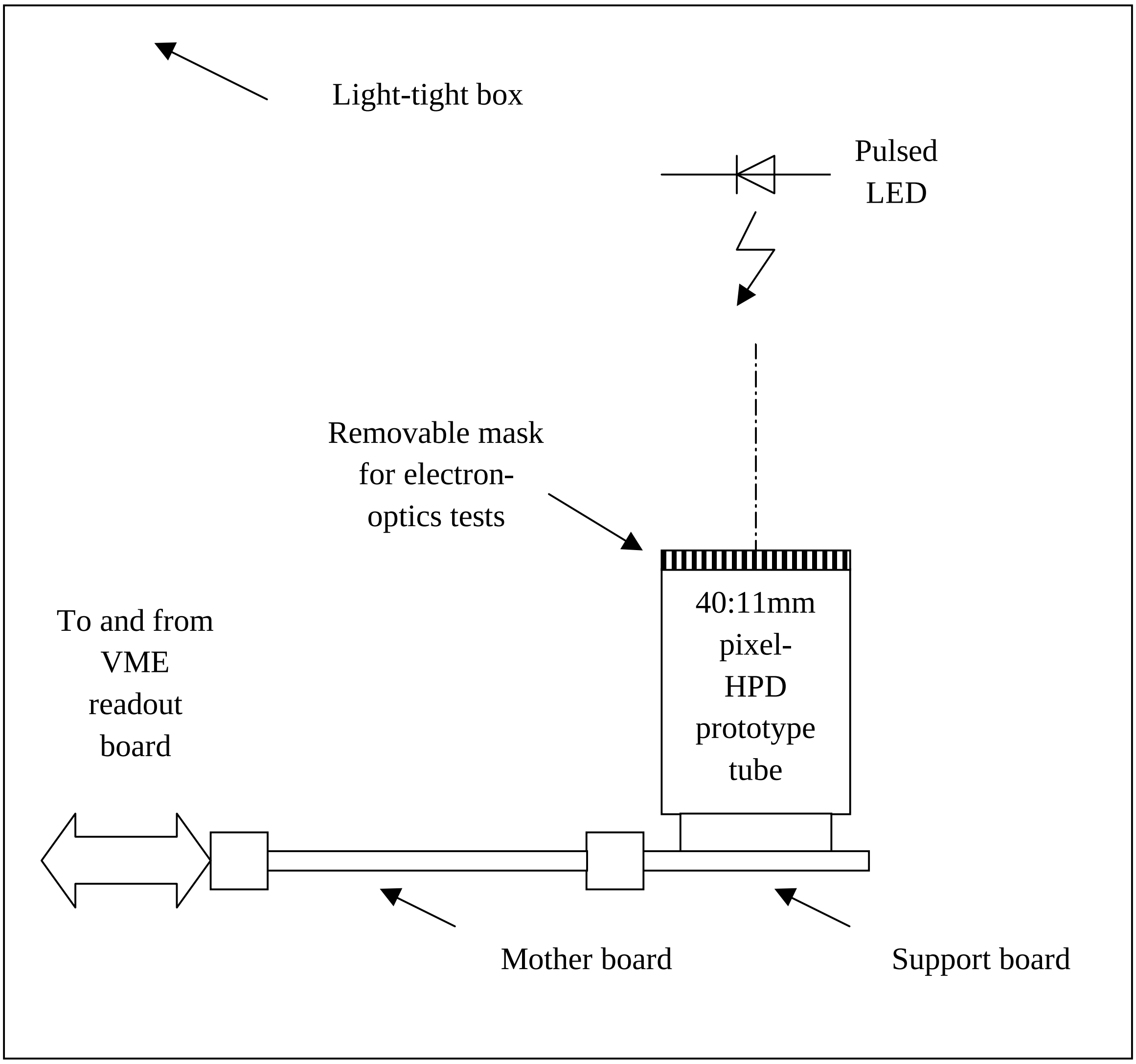
Light-tight box
Pulsed LED
Removable mask for electron-optics tests
40:11mm pixel-HPD prototype tube
To and from VME readout board
Mother board
Support board

Figure 7

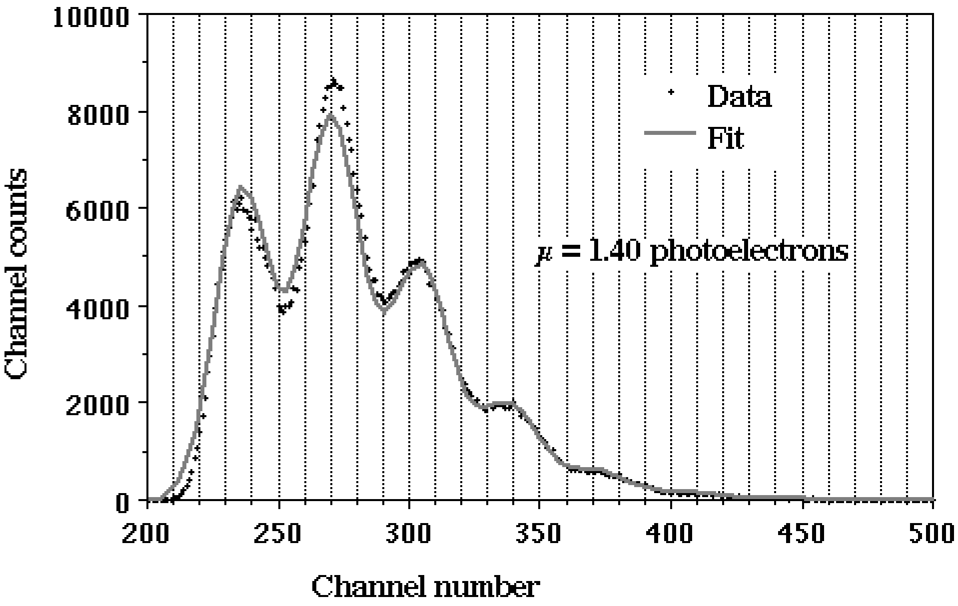
10000
8000
6000
4000
2000
0
Channel counts
200
250
300
350
400
450
500
Channel number
Data
Fit
μ = 1.40 photoelectrons

Figure 8

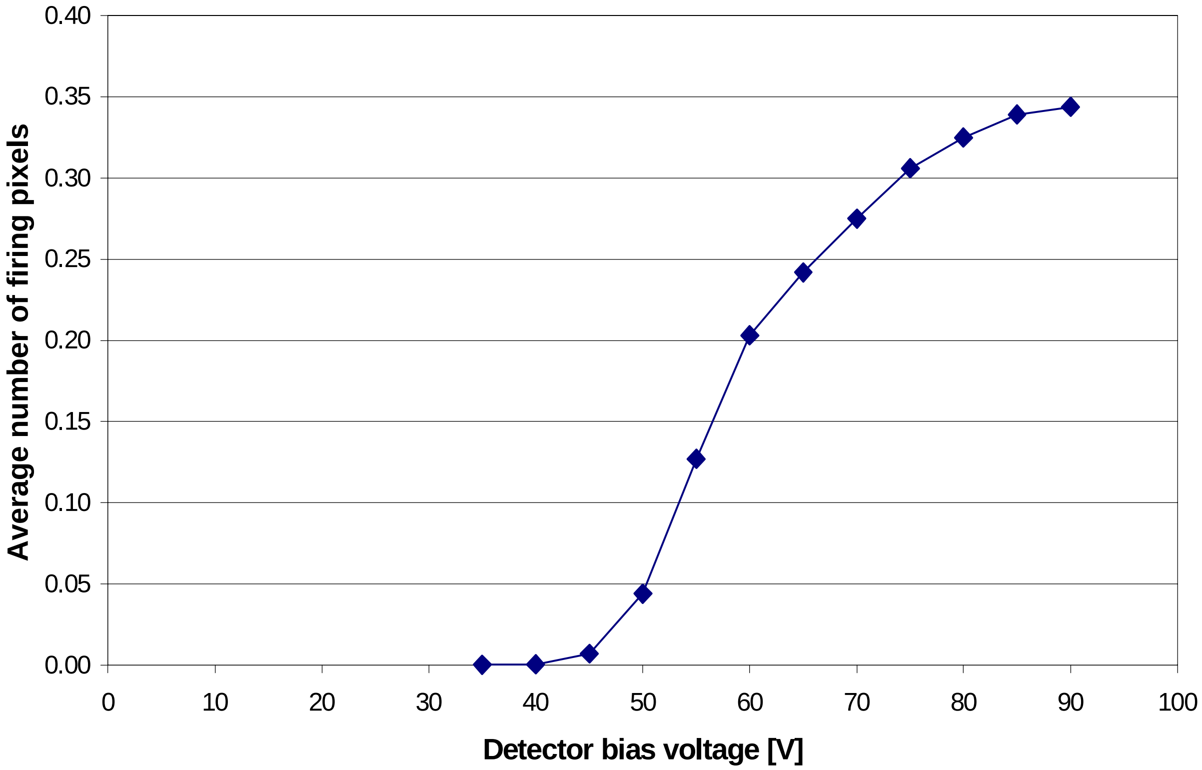
0.40
0.35
0.30
0.25
0.20
0.15
0.10
0.05
0.00
0
10
20
30
40
50
60
70
80
90
100
Average number of firing pixels
Detector bias voltage [V]

Figure 9

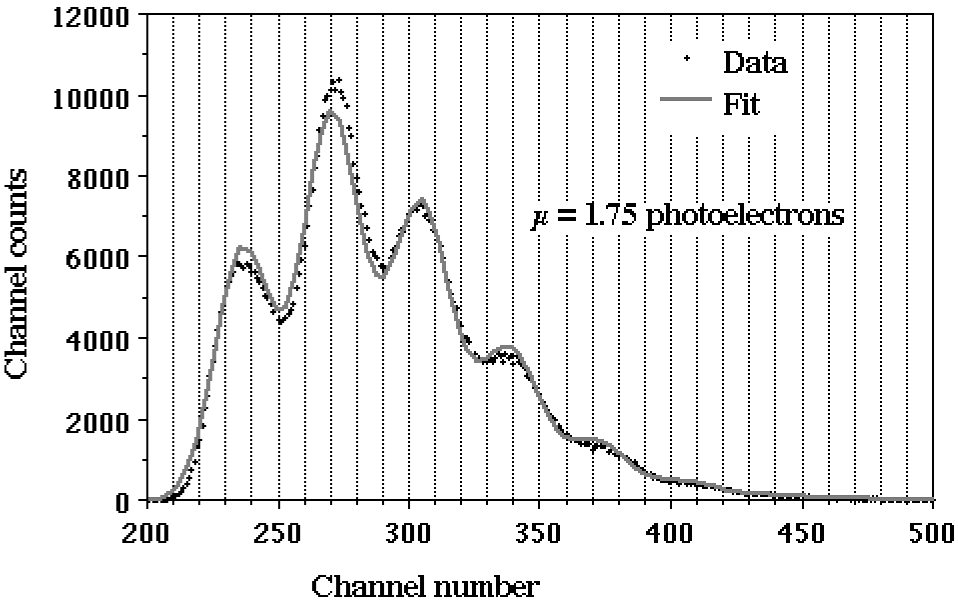
12000
10000
8000
6000
4000
2000
0
Channel counts
200
250
300
350
400
450
500
Channel number
Data
Fit
μ = 1.75 photoelectrons

Figure 10

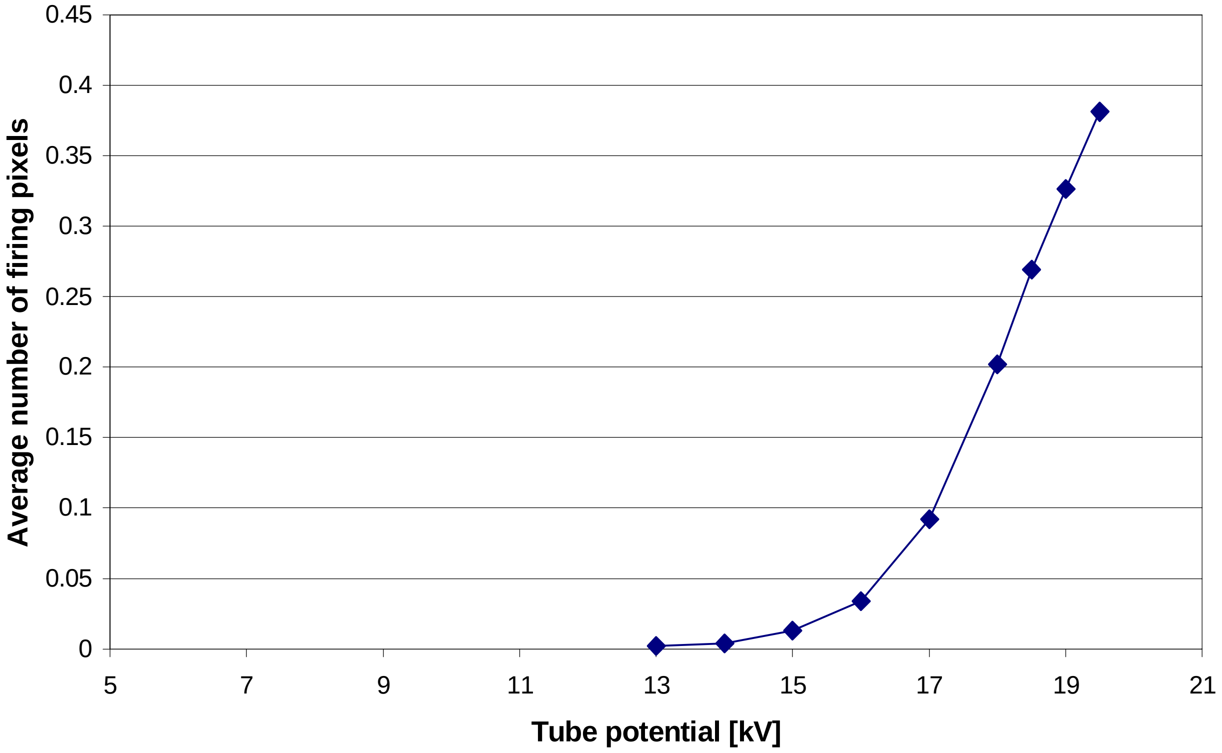
Average number of firing pixels
0.45
0.4
0.35
0.3
0.25
0.2
0.15
0.1
0.05
0
5
7
9
11
13
15
17
19
21
Tube potential [kV]

Figure 11

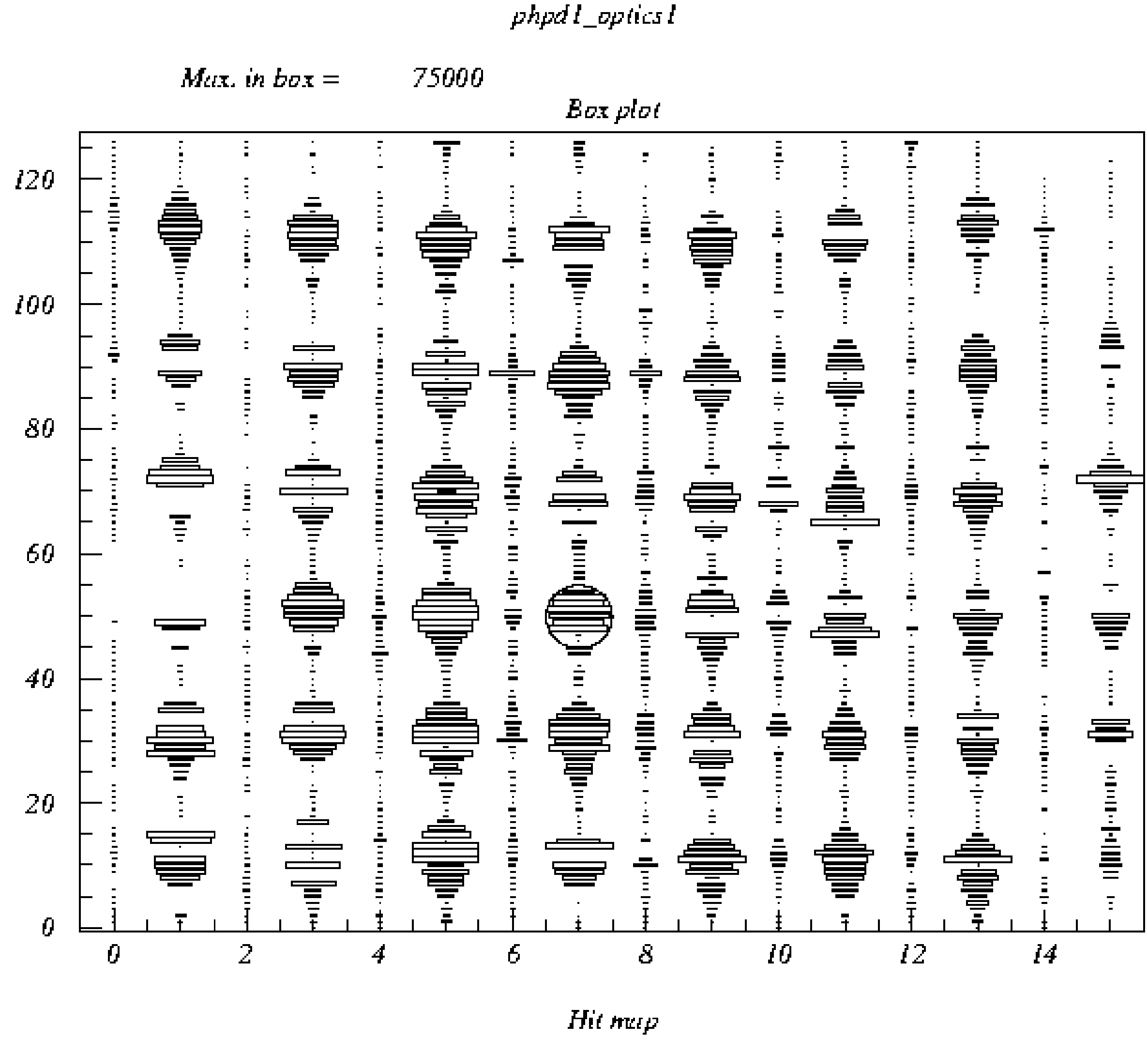
phpd1_optics1
Max. in box = 75000
Box plot
120
100
80
60
40
20
0
0
2
4
6
8
10
12
14
Hit map

Figure 12

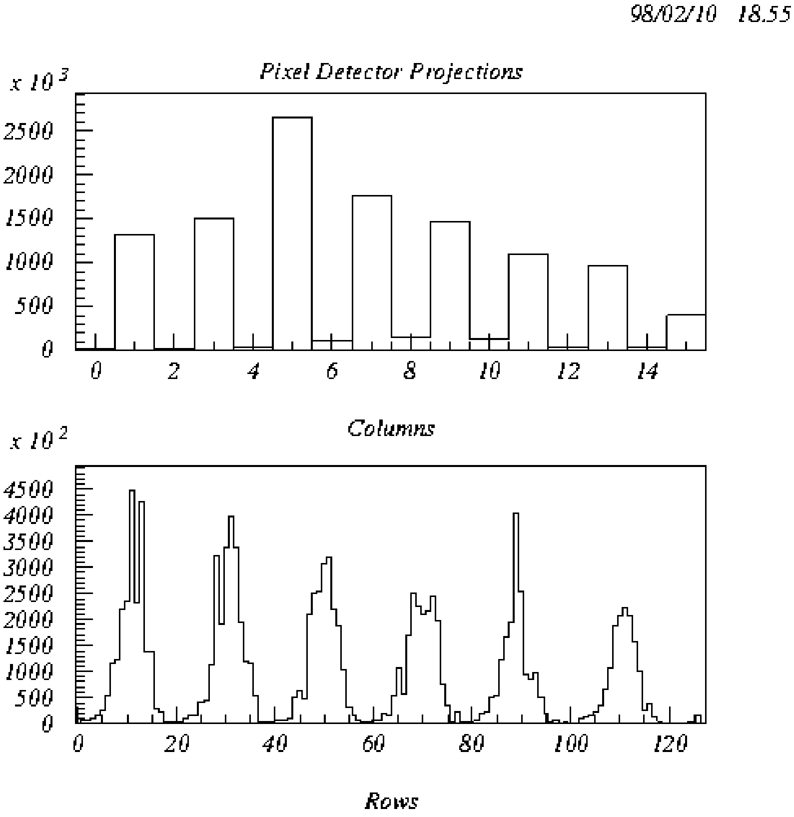
98/02/10 18.55
Pixel Detector Projections
x 10 3
2500
2000
1500
1000
500
0
0
2
4
6
8
10
12
14
Columns
x 10 2
4500
4000
3500
3000
2500
2000
1500
1000
500
0
0
20
40
60
80
100
120
Rows

Figure 13

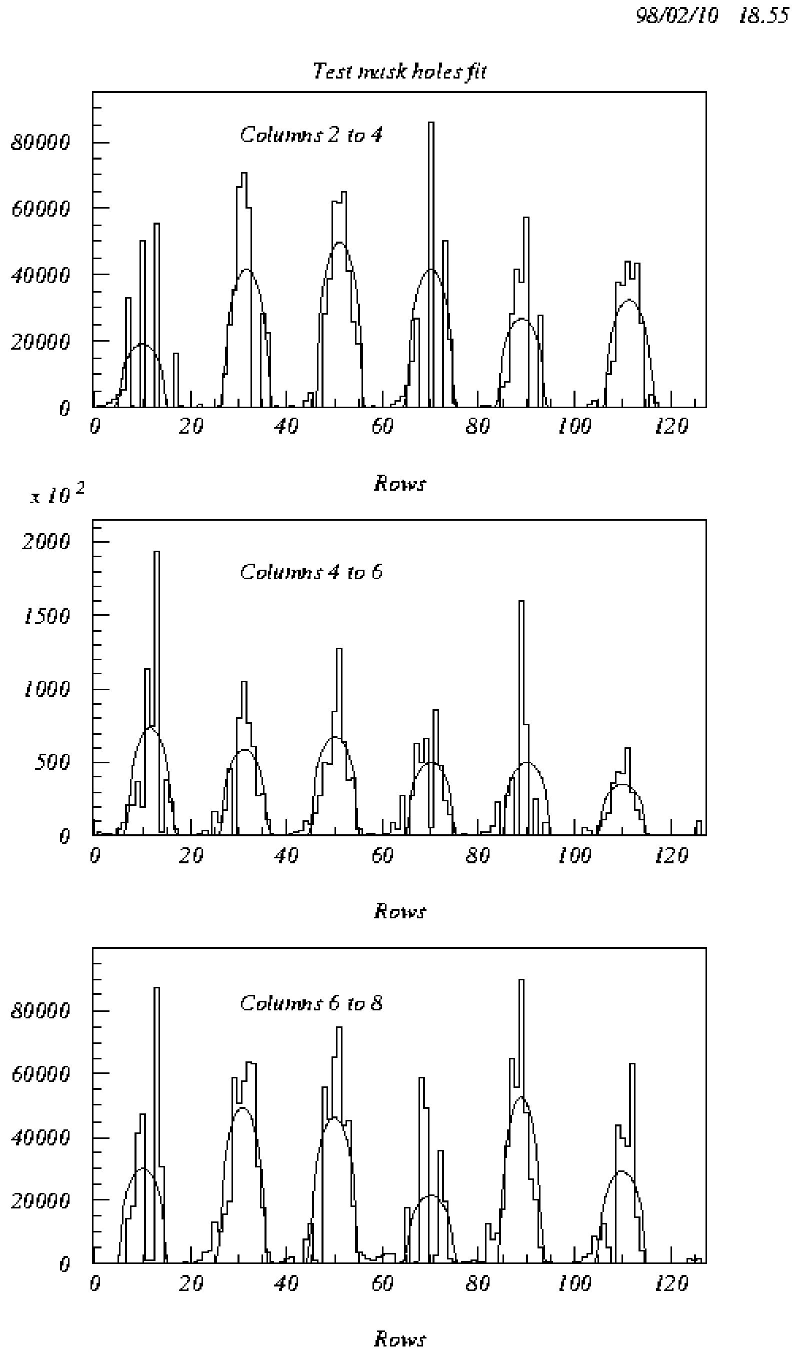
98/02/10 18.55
Test mask holes fit
Columns 2 to 4
80000
60000
40000
20000
0
0
20
40
60
80
100
120
Rows
x 10 2
Columns 4 to 6
2000
1500
1000
500
0
0
20
40
60
80
100
120
Rows
Columns 6 to 8
80000
60000
40000
20000
0
0
20
40
60
80
100
120
Rows

Figure 14

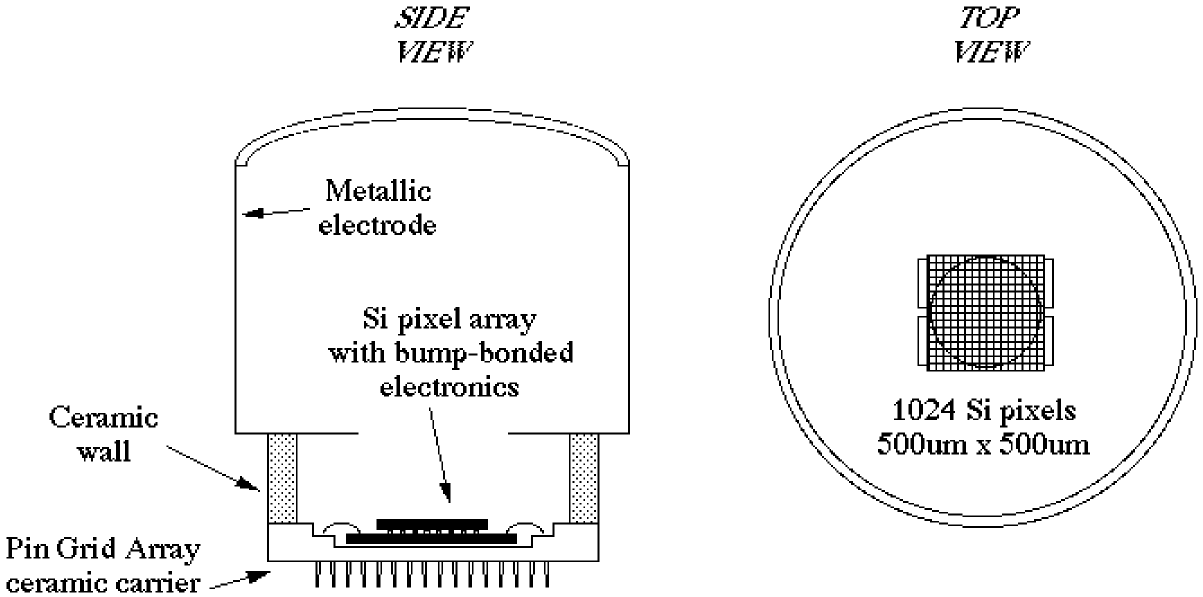
SIDE VIEW
TOP VIEW
Metallic electrode
Si pixel array with bump-bonded electronics
Ceramic wall
Pin Grid Array ceramic carrier
1024 Si pixels 500um x 500um

Figure 15

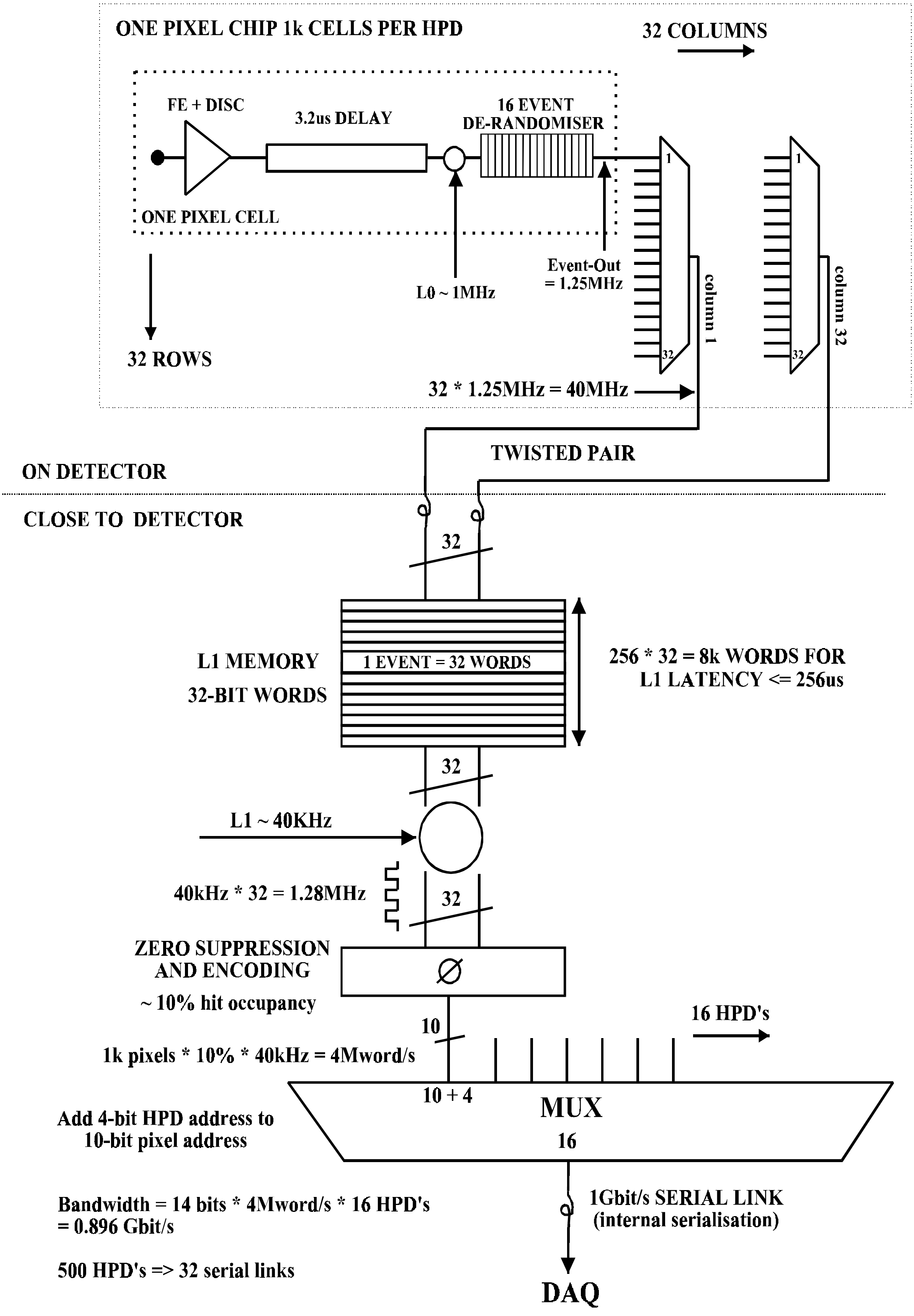
ONE PIXEL CHIP 1k CELLS PER HPD
32 COLUMNS
FE + DISC
3.2us DELAY
16 EVENT
DE-RANDOMISER
ONE PIXEL CELL
1
32
column 1
column 32
Event-Out
= 1.25MHz
L0 ~ 1MHz
32 ROWS
32 * 1.25MHz = 40MHz
TWISTED PAIR
ON DETECTOR
CLOSE TO DETECTOR
32
L1 MEMORY
32-BIT WORDS
1 EVENT = 32 WORDS
256 * 32 = 8k WORDS FOR
L1 LATENCY <= 256us
32
L1 ~ 40KHz
40kHz * 32 = 1.28MHz
32
ZERO SUPPRESSION
AND ENCODING
~ 10% hit occupancy
Ø
10
1k pixels * 10% * 40kHz = 4Mword/s
16 HPD's
10 + 4
MUX
16
Add 4-bit HPD address to
10-bit pixel address
Bandwidth = 14 bits * 4Mword/s * 16 HPD's
= 0.896 Gbit/s
500 HPD's => 32 serial links
1Gbit/s SERIAL LINK
(internal serialisation)
DAQ

Figure 16